

Article

Optimal Design of Ceramic Based Hip Implant Composites Using Hybrid AHP-MOORA Approach

Tej Singh ¹, Chandramani Goswami ², Amar Patnaik ³ and László Lendvai ^{4,*}

¹ Savaria Institute of Technology, Faculty of Informatics, Eötvös Loránd University, 9700 Szombathely, Hungary; sht@inf.elte.hu

² Department of Mechanical Engineering, Arya College of Engineering and Information Technology, Jaipur 302028, India; chandramani.goswami10@gmail.com

³ Department of Mechanical Engineering, Malaviya National Institute of Technology, Jaipur 302017, India; apatnaik.mech@mnit.ac.in

⁴ Department of Materials Science and Engineering, Széchenyi István University, 9026 Győr, Hungary

* Correspondence: lendvai.laszlo@sze.hu

Abstract: Designing excellent hip implant composite material with optimal physical, mechanical and wear properties is challenging. Improper hip implant composite design may result in a premature component and product failure. Therefore, a hybrid decision-making tool was proposed to select the optimal hip implant composite according to several criteria that are probably conflicting. In varying weight proportions, a series of hip implant composite materials containing different ceramics (magnesium oxide, zirconium oxide, chromium oxide, silicon nitride and aluminium oxide) were fabricated and evaluated for wear and physicochemical properties. The density, void content, hardness, indentation depth, elastic modulus, compressive strength, wear, and fracture toughness values were used to rank the hip implant composites. It was found that the density and void content of the biocomposites remain in the range of 3.920–4.307 g/cm³ and 0.0021–0.0089%, respectively. The composite without zirconium oxide exhibits the lowest density (3.920 g/cm³), while the void content remains lowest for the composite having no chromium oxide content. The highest values of hardness (28.81 GPa), elastic modulus (291 GPa) and fracture toughness (11.97 MPa.m^{1/2}) with the lowest wear (0.0071 mm³/million cycles) were exhibited by the composites having 83 wt.% of aluminium oxide and 10 wt.% of zirconium oxide. The experimental results are compositional dependent and without any visible trend. As a result, selecting the best composites among a group of composite alternatives becomes challenging. Therefore, a hybrid AHP-MOORA based multi-criteria decision-making approach was adopted to choose the best composite alternative. The AHP (analytic hierarchy process) was used to calculate the criteria weight, and MOORA (multiple objective optimisation on the basis of ratio analysis) was used to rank the composites. The outcomes revealed that the hip implant composite with 83 wt.% aluminium oxide, 10 wt.% zirconium oxide, 5 wt.% silicon nitride, 3 wt.% magnesium oxide, and 1.5 wt.% chromium oxide had the best qualities. Finally, sensitivity analysis was conducted to determine the ranking's robustness and stability concerning the criterion weight.

Keywords: hip implant composites; ceramic; physicochemical; AHP-MOORA; optimisation



Citation: Singh, T.; Goswami, C.; Patnaik, A.; Lendvai, L. Optimal Design of Ceramic Based Hip Implant Composites Using Hybrid AHP-MOORA Approach. *Materials* **2022**, *15*, 3800. <https://doi.org/10.3390/ma15113800>

Academic Editor: Philippe Colombari

Received: 7 April 2022

Accepted: 23 May 2022

Published: 26 May 2022

Publisher's Note: MDPI stays neutral with regard to jurisdictional claims in published maps and institutional affiliations.



Copyright: © 2022 by the authors. Licensee MDPI, Basel, Switzerland. This article is an open access article distributed under the terms and conditions of the Creative Commons Attribution (CC BY) license (<https://creativecommons.org/licenses/by/4.0/>).

1. Introduction

Over one million knee and hip replacements are performed each year, providing patients with improved mobility, pain relief, and personal satisfaction. According to reports, approximately 3.48 million knee replacements will be necessary by 2030, representing a 673 percent increase over the current number of treatments [1,2]. Total hip replacement is one of the best orthopaedic surgeries and has been widely used for re-establishing mobility to hip joints for decades; however, design-related complexities remain a concerning reason for implant failure [3,4]. Today, the main challenges faced by the designers are selecting

the proper raw materials in the right amounts, and the design of hip implant composites with excellent mechanical properties with higher wear resistance and biocompatibility [5,6]. For achieving these properties, various material combinations of metals, polymers and ceramics are reported for hip implant applications [7]. In particular, ceramic-on-ceramic-based hip implant composites have received much attention and are becoming increasingly important because of their unique properties, such as higher fracture toughness and wear resistance with excellent chemical stability compared to metal and polymer-based hip implant composites [8].

In 1970, aluminium oxide was the first ceramic material utilised in complete hip arthroplasty [9,10]. However, aluminium oxide leads to catastrophic failure due to its brittle nature [11]. The failure risk can be avoided by introducing zirconium oxide into an aluminium oxide matrix, resulting in a hip implant composite material with higher fracture toughness and reduced wear resistance and hardness [12,13]. To compensate for the hardness and wear resistance loss induced by the presence of zirconia, a tiny proportion of chromium oxide was added [14]. Magnesium oxide was reported to prevent the increase of aluminium oxide grain size during sintering [15]. A homogenous and denser microstructure can be obtained with magnesium oxide, which helps impart strength with increased wear resistance [16]. Zhang et al. [17] studied the influence of magnesium oxide on the mechanical properties and chemical stability of Ce-TZP/ Al_2O_3 based artificial joint materials. They found that with 0.2 wt.% magnesium oxide content, the various mechanical properties like flexural strength, hardness, and fracture toughness are the best and that it may be employed as a wear-resistant joint replacement material. Several researchers believe silicon nitride could be utilised in hip implant applications due to its higher chemical stability, and favourable mechanical and wear qualities [18].

Ceramic-based hip implant composites are gaining popularity due to their superior properties of mechanical (elastic modulus hardness, fracture toughness), high wear and corrosion resistance, and excellent biochemical stability and biocompatibility [10–18]. According to the literature, the hardness and strength of ceramic materials such as stabilized zirconium oxide reduced dramatically in water-containing conditions [19]. According to the research, the tetragonal to monoclinic transformation of zirconium oxide is the primary cause of ageing, leading to micro-cracks exacerbated in water vapours [19,20]. The phase transformation further promotes surface roughening, and grain pull out may result in the harmful effect of implanted components [21,22]. When a composite is embedded in the human body, it is well known that it causes several biological reactions. The poor biocompatibility of the implanted materials may result in bacterial infections along with the interface of bone and implanted material, leading to replacements or re-surgeries of the implants [18]. Furthermore, the inserted implants emit ions due to their repeated interactions with the surrounding environment, resulting in a decrease in the performance of the implanted component [23–26]. It is worth noting that the biochemical stability and biocompatibility of the produced ceramic composites have not been investigated in this current paper, although we understand that these properties are of great importance for end-user applications.

The ultimate performance of the intended hip implant composite depends upon the type and size of the used ingredients with appropriate manufacturing conditions. Hence, the proper attention is required to be paid to the compositional design [27,28]. Moreover, the developed hip implant composites have their own performance implications for the evaluated wear and physicomechanical properties [29]. As a result, selecting the appropriate composition with the desired sound qualities becomes a challenging task that can be accomplished using multi-criteria decision-making (MCDM) tools [30]. These are statistical methods used to tackle complex decision-making problems utilising a finite number of qualities and options [31]. MCDM approaches include AHP (analytic hierarchy process), MOORA (multiple objective optimisation on the basis of ratio analysis), TOPSIS (a technique for the ordering of preference by similarity to ideal solution), VIKOR (vise kriterijumska optimizacija kompromisno resenje), MABAC (multi-attributive border ap-

proximation area comparison), SAW (simple additive weighting), MEW (multiplicative exponent weighting), and COPRAS (complex proportional assessment) have been effectively deployed to tackle a variety of decision-making problems [32–37]. Among them, MOORA and AHP are very popular. MOORA method is straightforward to understand and implement as it requires significantly fewer computations. The AHP technique, on the other hand, was utilised to determine the relative importance or weight of the criterion employed in various ranking procedures. These approaches are appropriate for decision-making problems and have been successfully implemented in many fields [38,39]. Therefore, in this paper, after manufacturing a series of hip implant composites with varying content of different ceramics and assessing their physical, mechanical, and wear properties, a hybrid AHP-MOORA methodology is proposed for ranking. The main objective is to choose an ideal hip implant composite with the MOORA method, which AHP strengthens for the estimation of criterion weight.

2. Experimental Methodology

2.1. Materials and Hip Implant Composite Fabrication

Magnesium oxide (MgO), zirconium oxide (ZrO_2), chromium oxide (Cr_2O_3), silicon nitride (Si_3N_4) and aluminum oxide (Al_2O_3) were purchased from Daisy Impex Chemicals (Average particle size = 0.2–5 μm ; New Delhi, India).

The spark plasma sintering (SPS) procedure was used to create samples with varying weight percentages of selected ceramic materials, as shown in Table 1. First, the selected ceramic materials were milled for 4 h at 300 rpm in a toluene solution (50 mL) using a grinding medium (tungsten). The mixture of powders was separated from the solution by filtration through fine filter paper, and then oven dried. Then, in a vacuum, samples sized 10 mm (in thickness) and 20 mm (in diameter) were sintered using SPS-725 equipment from DR. SINTER, Japan. The sets of prepared composite powder mixtures were carefully placed into a 20 mm diameter graphite die. A sheet of graphitic paper was placed between the punch and the powders and between the die and the powders for easy removal of the sintered sample. A pressure of 60 MPa was applied throughout the sintering cycle. The sintering temperature was increased to 1400 °C at a rate of 300 °C/min [40]. A 3 min holding time was used when the maximum temperature was reached. The polished samples (Figure 1) were then subjected to physical, mechanical, and wear tests.

Table 1. Compositional detail of hip implant composite alternatives.

Composition (wt.%)	Alternatives												
	A-1	A-2	A-3	A-4	A-5	A-6	A-7	A-8	A-9	A-10	A-11	A-12	A-13
Al_2O_3	72	71.25	70.5	69.75	73.5	72	69	75.5	73	68	93	83	63
ZrO_2	20	20	20	20	20	20	20	20	20	20	0	10	30
Si_3N_4	5	5	5	5	5	5	5	0	2.5	7.5	2.5	2.5	2.5
MgO	3	3	3	3	0	1.5	4.5	3	3	3	3	3	3
Cr_2O_3	0	0.75	1.5	2.25	1.5	1.5	1.5	1.5	1.5	1.5	1.5	1.5	1.5



Figure 1. Manufactured composite samples.

2.2. Measurements

The experimental density was calculated using Wensar density measurement equipment, whereas the mixture rule was used for void content determination. The nanoindentation test was carried out as per ASTM E2546 standard to determine Young's modulus and hardness properties of manufactured hip implant composites. For this, a Hysitron TI 750-D (Ubi-1 model) testing machine was used. The Berkovich diamond indenter was used with a 150 nm tip radius. The indentation time was 10 s, and the applied load was 5000 μN with a 500 $\mu\text{N/s}$ loading rate [41]. The load and associated penetration depth values were recorded. After that, Young's modulus and hardness were computed with the help of Pharr and Oliver's model [42]. On each composite sample, fifteen indents were made to increase the reliability of the data. The compression tests performed on a universal testing machine (Model No. 8862, INSTRON, High Wycombe, UK) on the manufactured composite samples with 1 mm/min cross-head speed. Fracture toughness of manufactured hip implant composites was computed by measuring the crack formed due to the Vickers indentation and half-penny crack system. Therefore, the manufactured composites were penetrated with the help of a hardness tester from Buehler, USA, for crack generation. The penetration time was 13 s, and the applied load was 20 N. The length of the generated crack was counted using a scanning electron microscope. Finally, the Anstis model was implemented to compute the fracture toughness (K_{IC}) as [43];

$$K_{IC} = 0.016 \left(\frac{Y}{H} \right)^{\frac{1}{2}} \times \frac{f}{c^{\frac{3}{2}}} \quad (1)$$

where, H = Hardness, Y = Young's modulus, f = Applied load; $c = a + l$, l = crack length, a = half diagonal of the indent.

To increase the accuracy of the obtained results, the experiments were repeated five times and the mean data were reported with the estimated error.

2.3. Wear Characterization

The manufactured hip implant composites were evaluated for wear behaviour on a ring-on-plate type tribometer (Ducom, India; model: TR-6474). The systematic of the machine is presented in Figure 2. The wear tests were conducted according to ISO 6474-1:2010 [44]. The tribometer's structure is built of mild steel. The structure's upper part is linked to a base plate. A support stand is welded to the base plate, and a crank mechanism is installed. A motor is mounted vertically on a welded support stand. The motor shaft is usually visible above the stand. To pivot alongside the shaft, a crank wheel is fixed to it. The wheel rotates the axle via a switch, oscillating the composite sample plate by 25 degrees while the base plate remains stationary. Sintered and polished composite samples were placed on the top plate and rotated at the selected frequency across an arc of 25° against a base plate. The base plate with dimensions of 25 mm (diameter) \times 6 mm (height) was selected from the manufactured composites. The base plate was manufactured using the same sintering procedure described in Section 2.1. Wear tests were carried out with a frequency of 50 Hz and 500 N load for one million cycles using simulated body fluid conditions as per ISO 23317 [45]. After the completion of the test, wear was computed on a volume basis according to Equation (2). For each composite, three samples were used for wear estimation, and average is reported.

$$K = \frac{w_2 - w_1}{\rho} \quad (2)$$

Here, w_1 = sample weight before test, w_2 = sample weight after test, ρ = sample density.

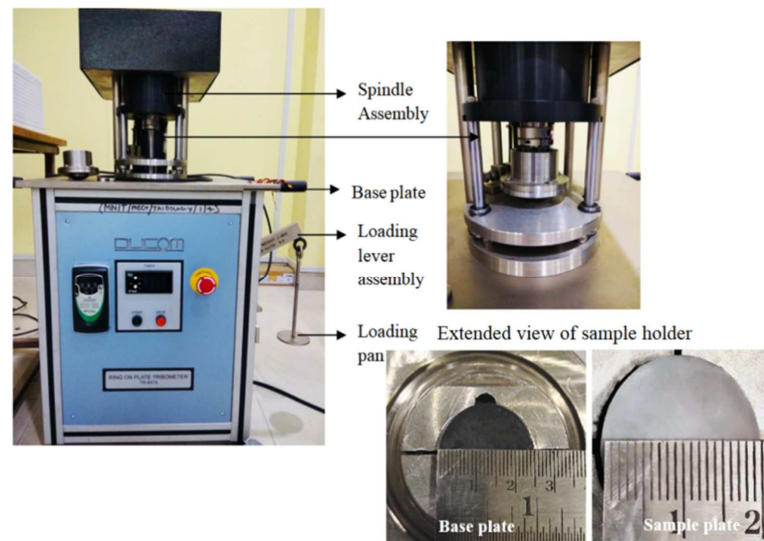


Figure 2. Ring on plate tribometer.

2.4. Determination and Implication of Criterion

The evaluated physical (density, void content), mechanical (hardness, elastic modulus, fracture toughness, and compressive strength) and wear properties were taken as a criterion in the ranking process of the developed hip implant composites. The implications of the selected criterion are given as:

- Criterion-1 (C-1): Density (g/cm^3 , Lower-is-better)
- Criterion-2 (C-2): Void content (Volume-%, Lower-is-better)
- Criterion-3 (C-3): Hardness (GPa, Higher-is-better)
- Criterion-4 (C-4): Indentation depth (nm, Lower-is-better)
- Criterion-5 (C-5): Elastic modulus (GPa, Higher-is-better)
- Criterion-6 (C-6): Fracture toughness ($\text{MPa}\cdot\text{m}^{1/2}$, Higher-is-better)
- Criterion-7 (C-7): Compressive strength (GPa, Higher-is-better)
- Criterion-8 (C-8): Wear ($\text{mm}^3/\text{million cycles}$, Lower-is-better)

2.5. Evaluation Methodology

The MCDM approaches are generally used to rank a predetermined number of alternatives considering a set of criteria. The various parts, namely criterion, alternatives, and performance matrix, of any MCDM approach are presented in Figure 3. The algorithm of this hybrid AHP-MOORA approach is systematically presented in Figure 4.

	Criterion				Ranking
	Criterion-1	Criterion-2	...	Criterion-n	
	Criterion weight				
	$\varpi-1$	$\varpi-2$...	$\varpi-n$	
Alternatives	Performance matrix				
Alternative-1	P_{11}	P_{12}	...	P_{1n}	Rank-1
Alternative-2	P_{21}	P_{22}	...	P_{2n}	Rank-2
...
Alternative-m	P_{m1}	P_{m2}	...	P_{mn}	Rank-m

Figure 3. A MCDM model.

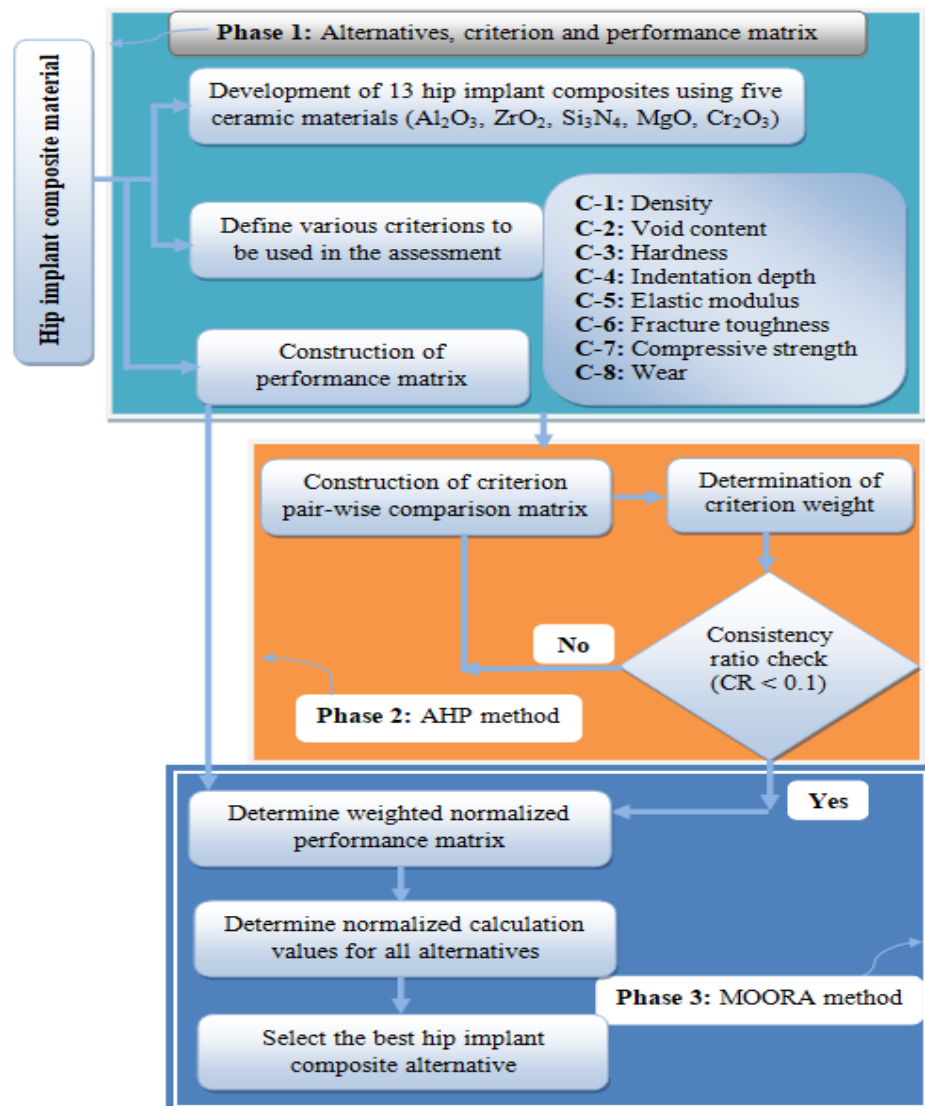


Figure 4. Architecture of the hybrid AHP-MOORA approach.

The proposed hybrid AHP-MOORA approach contains three phases, namely:

Phase 1: Alternatives, criterion and creation of performance matrix

Phase 2: AHP for criterion weight determination

Phase 3: MOORA approach for alternatives ranking

2.5.1. Phase 1: Alternatives, Criterion and Creation of Performance Matrix

In order to initiate any MCDM approach, the number of criteria and alternatives needs to be defined first. For selected alternatives (presented in Table 1) and criteria (described in Section 2.4), a performance matrix is generated as:

$$P_{m \times n} = \begin{matrix} & C_1 & C_j & \cdots & C_n \\ \begin{matrix} A_1 \\ A_i \\ \vdots \\ A_m \end{matrix} & \begin{bmatrix} p_{11} & p_{1j} & \cdots & p_{1n} \\ p_{i1} & p_{ij} & \cdots & p_{in} \\ \vdots & \vdots & \ddots & \vdots \\ p_{m1} & p_{mj} & \cdots & p_{mn} \end{bmatrix} \end{matrix} \quad (3)$$

where, the factor p_{ij} symbolizes the value of i^{th} alternative with respect to j^{th} criterion.

2.5.2. Phase 2: AHP for Criteria Weight Determination

For weight estimation, a pair-wise comparison matrix first structured using scale of 1 to 9 [46]. For n criteria $\{C - j; j = 1, 2, \dots, n\}$, the structured matrix (\hat{h}) is:

$$\hat{h}_{n \times n} = \begin{matrix} & C_1 & C_j & \dots & C_n \\ \begin{matrix} C_1 \\ C_k \\ \vdots \\ C_n \end{matrix} & \begin{bmatrix} h_{11} & h_{1j} & \dots & h_{1n} \\ h_{k1} & h_{kj} & \dots & h_{kn} \\ \vdots & \vdots & \ddots & \vdots \\ h_{n1} & h_{nj} & \dots & h_{nn} \end{bmatrix} \end{matrix} \tag{4}$$

where, h_{kj} is the comparative importance of k^{th} to j^{th} criteria. Diagonally the criteria values are self-compared, hence $h_{kj} = 1$, where $k = j; k, j = 1, 2 \dots n$.

By using geometric mean method, the criteria weight is computed as:

$$\varpi_i = \frac{\left(\prod_{j=1}^n h_{kj}\right)^{\frac{1}{n}}}{\sum_{i=1}^n \left(\prod_{j=1}^n h_{kj}\right)^{\frac{1}{n}}} \tag{5}$$

Finally, to ensure the stability of weight determined, consistency ratio (CR) is determined as:

$$CR = \frac{\lambda_{\max} - n}{RI \times (n - 1)} \tag{6}$$

Here, RI (random index) is the order value of the matrix [47] and λ_{\max} is the maximum Eigen value determined using the following equation:

$$\hat{h}_{n \times n} \times \varpi_i = \lambda_{\max} \times \varpi_i \tag{7}$$

2.5.3. Phase 3: MOORA Approach for Alternatives Ranking

Proposed by Brauers [48], the MOORA approach has successfully been applied in various decision-making problems [49,50]. In MOORA methodology, the constructed performance matrix is first normalized in between 0–1 by using the following equation:

$$p_{ij}^* = \frac{p_{ij}}{\sum_{i=1}^m p_{ij}^2} \tag{8}$$

Next, the weighted normalized performance matrix was constructed as:

$$N_{ij} = p_{ij}^* \times \varpi_j \tag{9}$$

Finally, the normalized values were added for favourable (higher-is-better) criteria and subtracted for non-favourable (lower-is-better) criteria as:

$$\Psi_i = \Psi_1 - \Psi_2 \tag{10}$$

$$\Psi_1 = \sum_{j=1}^{\alpha} N_{ij} \tag{11}$$

$$\Psi_2 = \sum_{j=\alpha+1}^n N_{ij} \tag{12}$$

where Ψ_i represents the computation of i^{th} alternative. The α and $n-\alpha$ values represent the favourable and non-favourable criteria. The final ranking of the alternatives is established by sorting the Ψ_i values in descending order.

3. Results and Discussion

3.1. Criteria Interpretation

The results of evaluated wear and physicochemical properties are presented in Table 2. The density of the manufactured composites remains in the range of 3.92 g/cm³ to 4.307 g/cm³. The alternative without ZrO₂ content, i.e., A-11, had the lowest density, and alternative A-13 with 30 wt.% ZrO₂ was highest. The alternative A-11 with 10 wt.% ZrO₂ content exhibits a density of 4.048 g/cm³, whereas for alternatives A-1 to A-10 with 20 wt.% ZrO₂ the densities fluctuate in between 4.166 ± 0.024 g/cm³. This trend in density may be ascribed to the presence of high dense ZrO₂ content. This increase in density with increased ZrO₂ content is correlated to its lower sintering temperatures in relation to Al₂O₃ content [51]. The lowest and highest void contents were observed for A-1 and A-5 alternatives, respectively. The void content of alternative A-5 without MgO added composite remains highest (0.0089%), whereas, for MgO based composites, it remains lower and fluctuates between 0.0021% and 0.0063%. It was accounted for that in a higher temperature sintering process, MgO transforms into liquids and attempts to fill the pores resulted in reduced void content [17]. The alternative A-12 had 83 wt.% Al₂O₃ content showed a minor indentation depth (63.25 nm) with the highest hardness values (28.81 GPa). The observed value of hardness was nearly 50% higher, and indentation depth was almost 28% lower than the values observed for alternatives A-1, A-5 and A-8, where they remain 19.32 ± 0.13 GPa and 81 ± 5 nm, respectively.

Table 2. Experimental results.

Alternatives	C-1	C-2	C-3	C-4	C-5	C-6	C-7	C-8
A-1	4.151 ± 0.001	0.0021	19.19 ± 0.68	79.03 ± 2.32	226.12 ± 6.85	04.19 ± 0.17	2.715 ± 0.07	0.0246 ± 0.0008
A-2	4.154 ± 0.002	0.0033	21.34 ± 1.07	72.92 ± 1.82	239.10 ± 6.29	04.85 ± 0.24	2.772 ± 0.07	0.0152 ± 0.0005
A-3	4.158 ± 0.002	0.0042	27.83 ± 1.16	69.61 ± 1.55	276.55 ± 9.88	11.41 ± 0.41	2.841 ± 0.07	0.0078 ± 0.0004
A-4	4.161 ± 0.001	0.0054	20.93 ± 0.88	73.68 ± 1.67	232.05 ± 5.53	04.90 ± 0.15	2.796 ± 0.07	0.0127 ± 0.0006
A-5	4.152 ± 0.001	0.0089	19.33 ± 0.76	86.03 ± 2.26	243.12 ± 6.57	05.75 ± 0.19	2.730 ± 0.08	0.0323 ± 0.0010
A-6	4.156 ± 0.002	0.0063	20.99 ± 0.84	82.92 ± 1.68	244.10 ± 4.88	07.84 ± 0.27	2.793 ± 0.04	0.0276 ± 0.0008
A-7	4.150 ± 0.002	0.0045	19.93 ± 0.72	87.68 ± 1.58	229.05 ± 4.16	05.87 ± 0.23	2.816 ± 0.03	0.0289 ± 0.0008
A-8	4.190 ± 0.001	0.0044	19.45 ± 0.61	76.14 ± 2.82	235.85 ± 5.24	08.63 ± 0.26	2.718 ± 0.05	0.0213 ± 0.0009
A-9	4.176 ± 0.002	0.0038	28.64 ± 1.10	67.93 ± 1.66	280.18 ± 6.83	11.84 ± 0.48	2.861 ± 0.05	0.0076 ± 0.0003
A-10	4.142 ± 0.003	0.0043	22.69 ± 0.71	72.18 ± 2.01	245.12 ± 4.71	09.93 ± 0.34	2.810 ± 0.06	0.0139 ± 0.0007
A-11	3.920 ± 0.002	0.0045	19.93 ± 0.22	79.74 ± 2.28	263.12 ± 7.97	08.47 ± 0.22	2.814 ± 0.06	0.0196 ± 0.0006
A-12	4.048 ± 0.002	0.0032	28.81 ± 0.96	63.25 ± 1.64	291.00 ± 9.72	11.97 ± 0.28	2.894 ± 0.06	0.0071 ± 0.0002
A-13	4.307 ± 0.002	0.0058	20.79 ± 0.72	78.83 ± 1.43	253.05 ± 7.23	07.45 ± 0.21	2.818 ± 0.05	0.0127 ± 0.0003

In the literature, the hardness of 18.3 GPa for MgO doped Ce-TZP/Al₂O₃, 18.70 ± 6.63 GPa for Si₃N₄-MgO, 19.6 ± 0.2 GPa for graphene oxide filled 3Y-ZrO₂, and 28±2 GPa for zirconia-toughened alumina-based ceramic composites were reported by Zhang et al. [17], Mazzocchi et al. [52], Zhang et al. [53] and Bull et al. [54], respectively. Comparatively, the highest hardness of 28.81 GPa with a minor indentation depth of 63.25 nm remains much higher than the results of Zhang et al. [17], Mazzocchi et al. [52] and Zhang et al. [53] and remains nearly the same as the results of Bull et al. [54]. The elastic modulus, fracture toughness, and compressive strength for the alternative A-3 remained 276.55 GPa, 11.41 MPa.m^{1/2} and 2.841 GPa. With an increase in Al₂O₃ content to 73 wt.% and a corresponding decrease in Si₃N₄ content to 2.5 wt.%, a small increment in elastic modulus, fracture toughness and compressive strength was observed for alternative A-9. Further increase in Al₂O₃ content to 83 wt.% with a corresponding decrease in ZrO₂ content to 10 wt.%, an increment of ~1–4% in elastic modulus (291 GPa), fracture toughness (11.97 MPa.m^{1/2}), and compressive strength (2.894 GPa) was registered and remained maximum for alternative A-12. Similar results of elastic modulus and fracture toughness was reported by Zhang

et al. [53] and Bull et al. [54] for graphene oxide filled 3Y-ZrO₂ and zirconia-toughened alumina-based ceramic composites. While studying the influence of MgO (0 to 0.3 wt.%) and Ce-TZP (5 to 25 vol.%) in MgO doped Ce-TZP/Al₂O₃ bioceramic-based composites, Zhang and co-workers [17] reported similar results for fracture toughness. As per [17], a significant improvement in fracture toughness was reported with increasing Ce-TZP concentration and remains maximum (12.10 MPa.m^{1/2}) with 20 vol.% of Ce-TZP and 0.2 wt.% of MgO content. Recently, Sedláč et al. [55] investigated the nanomechanical properties of spark plasma sintered (1400 °C) oxide ceramics (70 wt.% Al₂O₃ + 30 wt.% ZrO₂) composites using nanoindentation. A Berkovich diamond indenter with a continuous stiffness measuring mode with a strain rate of 0.05 s⁻¹ and 200 nm depth was used. The authors claimed a hardness of 29.5 GPa, elastic modulus of 337 GPa, and fracture toughness of 3.72 MPa.m^{1/2}. The highest experimental values of hardness and elastic modulus in the present work are close to the results of Sedláč et al. [55], whereas the highest fracture toughness was almost 3.2 times higher than the results reported in ref. [55].

The Al₂O₃-ZrO₂ are widely known as mechanically and biologically compatible ceramic materials [42]. The performance of the final composite depends upon the composition, and it was reported that the uniform distribution of ZrO₂ particles was greatly hampered in the Al₂O₃-based composites with their increased (>20 wt.%) concentration. These structural inhomogeneities could form large voids in the composite. A higher temperature is required to eliminate these voids, which could cause the unusual grain growth of Al₂O₃, having a detrimental impact on the mechanical and wear performance of the composites [56]. The inclusion of various ceramics is reported to alter the performance of Al₂O₃-ZrO₂ ceramic-based composites beneficially. It was reported that the addition of MgO resists the growth of Al₂O₃ grains due to the microstructure pinning effect [57,58]. The addition of Cr₂O₃ was reported to enhance the mechanical performance of Al₂O₃ as it increases crack bridging [59]. Furthermore, covalently bonded Si₃N₄ has much higher mechanical strength than well-known oxide bioceramics and has been reported to enhance the strength and wear performance of Al₂O₃-ZrO₂ based composites [60]. The wear remains 0.0078 mm³/million cycles for alternative A-3 having 70.50 wt.% and 5 wt.% Al₂O₃ and Si₃N₄. A reduction of nearly 3% in wear was reported for alternative A-9 by increasing Al₂O₃ content to 73 wt.% and decreasing Si₃N₄ content to 2.5 wt.%. Further reduction in wear was observed for alternative A-12 (0.0071 mm³/million cycles) by increasing Al₂O₃ content to 83 wt.% and decreasing ZrO₂ content to 10 wt.%. The observed trends for the wear rate of manufactured composites were consistent with the reported range of implant composites. In the literature, the wear rate of 0.01–0.1 mm³ per million cycles was reported for alumina-on-alumina implants by Gallo et al. [61], 0.0036 mm³ per million cycles for polycrystalline diamond-based materials by Harding et al. [62] and 0.005 mm³ per million cycles for nanocrystalline diamond-coated ceramic hip joints by Amaral and co-workers [63]. The lowest wear rate of 0.0071 mm³ per million-cycles for alternative A-12 remained much lower than the results of alumina-on-alumina implants [61] but remained nearly 30 to 49% higher than the results of polycrystalline diamond [62] and nanocrystalline diamond-coated implants [63].

The assessed criteria play a decisive role in designing successful hip implant materials. Lower experimental values are desirable for many criteria like density, void content, and wear, whereas higher values are desirable for hardness, indentation depth, elastic modulus, fracture toughness, and compressive strength. As shown in Table 3, no alternative can yield preferred lower and higher values for all criteria at a single time. Accordingly, to pick the best choice by considering all the criteria together, a hybrid AHP-MOORA approach was implemented.

Table 3. Pair-wise matrix for weight determination.

	C-1	C-2	C-3	C-4	C-5	C-6	C-7	C-8
C-1	1	1.5	0.5	0.67	0.33	0.25	0.67	0.17
C-2	0.67	1	0.25	0.5	0.2	0.17	0.33	0.13
C-3	2	4	1	1.5	2	0.33	1.50	0.25
C-4	1.5	2	0.67	1	0.67	0.25	0.5	0.2
C-5	3	5	0.5	1.5	1	0.5	2	0.33
C-6	4	6	3	4	2	1	4	0.5
C-7	1.50	3	0.67	2	0.5	0.25	1	0.2
C-8	6	8	4	5	3	2	5	1

3.2. Ranking of Alternative

3.2.1. Weight Calculation

The weights of the selected criteria were determined using the AHP approach. To begin, the criteria were compared using a pair-wise matrix, as shown in Table 3. The results of the AHP technique are shown in Table 4. The criteria weight order is the following: C-8 (0.340) > C-6 (0.227) > C-5 (0.111) > C-3 (0.108) > C-7 (0.074) > C-4 (0.062) > C-1 (0.048) > C-2 (0.030). Moreover, the CR value was determined as 0.023, which is lower than the prescribed limit of 0.1. Therefore, the computed weights were consistent and further utilised to rank the alternatives.

Table 4. Results of AHP method.

Criterion	Weight (w_i)	Consistency Parameters	
C-1	0.048	$\lambda_{\max} = 8.23$ CI = 0.033 RI = 1.41	CR = 0.023
C-2	0.030		
C-3	0.108		
C-4	0.062		
C-5	0.111		
C-6	0.227		
C-7	0.074		
C-8	0.340		

3.2.2. Ranking Analysis

Table 2 shows the experimental results of the researched hip implant composites, which were used as a performance matrix. Because each alternative produces a different result for each criterion, the performance matrix values were normalized in the range of 0–1 using Equation (8). Table 5 displays the normalized performance matrix. Following normalization, a weighted normalized matrix is created using Equation (9) and shown in Table 6. After weighted normalization, the value of each alternative is determined using Equations (10)–(12) and presented in Table 6. The value of the composite A-12 is the highest (0.1187), indicating that it is the best of all the possible options. The composites A-9 (0.1111) and A-3 (0.1111) come in second and third, respectively (0.1042). The composite A-5 demonstrates the least preference with a value of -0.0834. The ranking results are summarized in Table 6 and illustrated in Figure 5. Overall, the hip implant composites ranking in downward order is A-12, A-9, A-3, A-10, A-13, A-4, A-11, A-2, A-8, A-6, A-1, A-7 and A-5. This investigation revealed that the composite A-12, which contains 73 weight percent Al_2O_3 , 20 weight percent ZrO_2 , 2.5 weight percent Si_3N_4 , 2.5 weight percent Cr_2O_3 , and 3 weight percent MgO had the best combination of wear and physicochemical properties.

Table 5. Normalized performance matrix.

Alternatives	C-1	C-2	C-3	C-4	C-5	C-6	C-7	C-8
A-1	0.2778	0.1167	0.2358	0.2867	0.2494	0.1390	0.2691	0.3465
A-2	0.2780	0.1833	0.2623	0.2645	0.2637	0.1609	0.2747	0.2141
A-3	0.2783	0.2333	0.3420	0.2525	0.3050	0.3786	0.2815	0.1099
A-4	0.2785	0.3000	0.2572	0.2673	0.2560	0.1626	0.2771	0.1789
A-5	0.2779	0.4944	0.2376	0.3121	0.2682	0.1908	0.2705	0.4549
A-6	0.2781	0.3500	0.2580	0.3008	0.2692	0.2602	0.2768	0.3887
A-7	0.2777	0.2500	0.2449	0.3181	0.2526	0.1948	0.2791	0.4070
A-8	0.2804	0.2444	0.2390	0.2762	0.2601	0.2864	0.2693	0.3000
A-9	0.2795	0.2111	0.3520	0.2464	0.3090	0.3929	0.2835	0.1070
A-10	0.2772	0.2389	0.2789	0.2618	0.2704	0.3295	0.2785	0.1958
A-11	0.2623	0.2500	0.2449	0.2893	0.2902	0.2811	0.2789	0.2761
A-12	0.2709	0.1778	0.3541	0.2294	0.3210	0.3972	0.2868	0.1000
A-13	0.2882	0.3222	0.2555	0.2860	0.2791	0.2472	0.2793	0.1789

Table 6. Weighted matrix and ranking of alternatives.

Alternatives	Weighted Matrix								Ranking of Alternatives			
	C-1	C-2	C-3	C-4	C-5	C-6	C-7	C-8	Ψ_1	Ψ_2	Ψ_i	Ranking
A-1	0.0133	0.0035	0.0255	0.0178	0.0277	0.0316	0.0199	0.1178	0.1046	0.1524	-0.0478	11
A-2	0.0133	0.0055	0.0283	0.0164	0.0293	0.0365	0.0203	0.0728	0.1145	0.1080	0.0064	8
A-3	0.0134	0.0070	0.0369	0.0157	0.0339	0.0860	0.0208	0.0374	0.1776	0.0734	0.1042	3
A-4	0.0134	0.0090	0.0278	0.0166	0.0284	0.0369	0.0205	0.0608	0.1136	0.0998	0.0139	6
A-5	0.0133	0.0148	0.0257	0.0193	0.0298	0.0433	0.0200	0.1547	0.1188	0.2022	-0.0834	13
A-6	0.0134	0.0105	0.0279	0.0186	0.0299	0.0591	0.0205	0.1322	0.1373	0.1747	-0.0374	10
A-7	0.0133	0.0075	0.0265	0.0197	0.0280	0.0442	0.0207	0.1384	0.1194	0.1789	-0.0596	12
A-8	0.0135	0.0073	0.0258	0.0171	0.0289	0.0650	0.0199	0.1020	0.1396	0.1399	-0.0003	9
A-9	0.0134	0.0063	0.0380	0.0153	0.0343	0.0892	0.0210	0.0364	0.1825	0.0714	0.1111	2
A-10	0.0133	0.0072	0.0301	0.0162	0.0300	0.0748	0.0206	0.0666	0.1555	0.1033	0.0523	4
A-11	0.0126	0.0075	0.0265	0.0179	0.0322	0.0638	0.0206	0.0939	0.1431	0.1319	0.0112	7
A-12	0.0130	0.0053	0.0382	0.0142	0.0356	0.0902	0.0212	0.0340	0.1853	0.0666	0.1187	1
A-13	0.0138	0.0097	0.0276	0.0177	0.0310	0.0561	0.0207	0.0608	0.1354	0.1020	0.0333	5

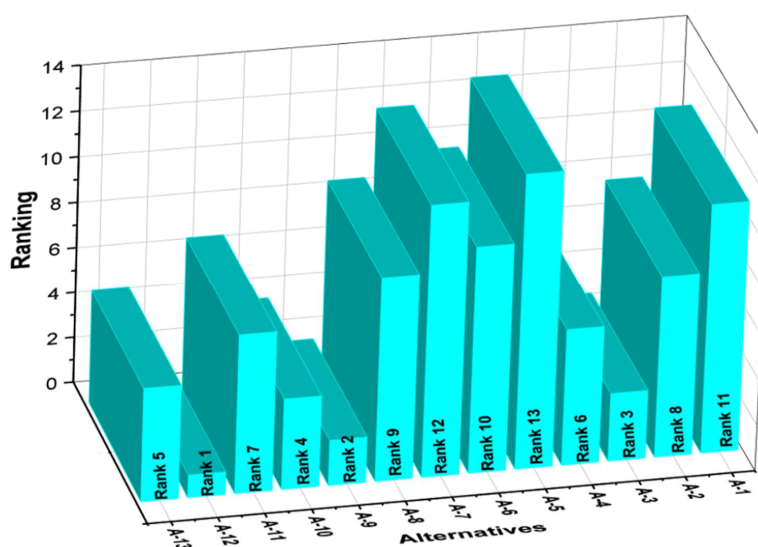


Figure 5. Ranking of hip implant alternatives.

3.3. Sensitivity Analysis

Furthermore, a sensitivity analysis was conducted to assess the ranking findings' robustness and stability in relation to the chosen criterion weight. This sensitivity analysis has been carried out by changing the weight of the two critical criteria, namely fracture toughness (C-6) and wear (C-8), the most weighted criteria with weights of 0.227 and 0.340, respectively, among the selected eight criteria. The sensitivity analysis was executed by increasing and decreasing a criterion weight in three steps ($\pm 5\%$, $\pm 10\%$ and $\pm 15\%$). The remaining seven criterion weights were adjusted proportionately to maintain the sum of all criterion weights equal to one. Tables 7 and 8 show the ranking of produced ceramic hip implant composites based on changes in the weight of selected criteria C-6 and C-8.

Table 7. Weight sensitivity of C-6 (fracture toughness) on ranking.

Alternatives	Weight Level						
	−15%	−10%	−5%	Original	+5%	+10%	+15%
	Ψ_i Value (Ranking)						
A-1	−0.0538 (11)	−0.0517 (11)	−0.0497 (11)	−0.0477 (11)	−0.0457 (11)	−0.0437 (11)	−0.0416 (11)
A-2	0.0003 (8)	0.0024 (8)	0.0045 (8)	0.0065 (8)	0.0086 (8)	0.0106 (8)	0.0127 (8)
A-3	0.0917 (3)	0.0959 (3)	0.1001 (3)	0.1043 (3)	0.1086 (3)	0.1128 (3)	0.1170 (3)
A-4	0.0072 (6)	0.0095 (6)	0.0117 (6)	0.0139 (6)	0.0162 (6)	0.0184 (7)	0.0206 (7)
A-5	−0.0936 (13)	−0.0901 (13)	−0.0867 (13)	−0.0833 (13)	−0.0800 (13)	−0.0766 (13)	−0.0731 (13)
A-6	−0.0487 (10)	−0.0448 (10)	−0.0411 (10)	−0.0373 (10)	−0.0335 (10)	−0.0297 (10)	−0.0259 (10)
A-7	−0.0685 (12)	−0.0654 (12)	−0.0625 (12)	−0.0595 (12)	−0.0565 (12)	−0.0535 (12)	−0.0505 (12)
A-8	−0.0116 (9)	−0.0078 (9)	−0.0040 (9)	−0.0002 (9)	0.0036 (9)	0.0074 (9)	0.0112 (9)
A-9	0.0983 (2)	0.1026 (2)	0.1069 (2)	0.1112 (2)	0.1155 (2)	0.1198 (2)	0.1241 (2)
A-10	0.0404 (4)	0.0444 (4)	0.0484 (4)	0.0524 (4)	0.0564 (4)	0.0603 (4)	0.0643 (4)
A-11	0.0004 (7)	0.0041 (7)	0.0077 (7)	0.0113 (7)	0.0149 (7)	0.0185 (6)	0.0222 (6)
A-12	0.1051 (1)	0.1093 (1)	0.1135 (1)	0.1178 (1)	0.1220 (1)	0.1262 (1)	0.1305 (1)
A-13	0.0237 (5)	0.0270 (5)	0.0302 (5)	0.0334 (5)	0.0366 (5)	0.0399 (5)	0.0431 (5)

Table 8. Weight sensitivity of C-8 (wear) on ranking.

Alternatives	Weight Level						
	−15%	−10%	−5%	Original	+5%	+10%	+15%
	Ψ_i Value (Ranking)						
A-1	−0.0285 (11)	−0.0348 (11)	−0.0414 (11)	−0.0477 (11)	−0.0540 (11)	−0.0614 (11)	−0.0669 (11)
A-2	0.0191 (8)	0.0150 (8)	0.0106 (8)	0.0065 (8)	0.0024 (8)	−0.0028 (8)	−0.0060 (8)
A-3	0.1138 (3)	0.1108 (3)	0.1073 (3)	0.1043 (3)	0.1014 (3)	0.0971 (3)	0.0949 (3)
A-4	0.0238 (7)	0.0206 (7)	0.0172 (6)	0.0139 (6)	0.0107 (6)	0.0065 (6)	0.0041 (6)
A-5	−0.0610 (13)	−0.0685 (13)	−0.0758 (13)	−0.0833 (13)	−0.0908 (13)	−0.0991 (13)	−0.1057 (13)
A-6	−0.0165 (10)	−0.0234 (10)	−0.0304 (10)	−0.0373 (10)	−0.0442 (10)	−0.0520 (10)	−0.0581 (10)
A-7	−0.0378 (12)	−0.0450 (12)	−0.0523 (12)	−0.0595 (12)	−0.0667 (12)	−0.0748 (12)	−0.0811 (12)
A-8	0.0169 (9)	0.0113 (9)	0.0054 (9)	−0.0002 (9)	−0.0058 (9)	−0.0125 (9)	−0.0173 (9)
A-9	0.1209 (2)	0.1178 (2)	0.1142 (2)	0.1112 (2)	0.1082 (2)	0.1037 (2)	0.1015 (2)
A-10	0.0650 (4)	0.0609 (4)	0.0565 (4)	0.0524 (4)	0.0483 (4)	0.0430 (4)	0.0397 (4)
A-11	0.0275 (6)	0.0222 (6)	0.0166 (7)	0.0113 (7)	0.0060 (7)	−0.0003 (7)	−0.0048 (7)
A-12	0.1276 (1)	0.1245 (1)	0.1208 (1)	0.1178 (1)	0.1147 (1)	0.1102 (1)	0.1080 (1)
A-13	0.0437 (5)	0.0403 (5)	0.0368 (5)	0.0334 (5)	0.0300 (5)	0.0256 (5)	0.0231 (5)

The variation of C-6 and C-8 weights caused a little sensitivity in the composite ranking. However, within the range of $\pm 5\%$, $\pm 10\%$ and $\pm 15\%$, except for A-4 and A-11, all other composite alternatives retain their respective rankings irrespective of the weightage of the C-6 and C-8. As the weightage of C-6 is increased to +10% and +15%, the ranking of the alternative A-4 goes down by one place, and the ranking of A-11 goes up by one place. Similarly, as the weightage of C-8 is decreased to −10% and −15%, the ranking of

the alternative A-4 goes up by one place, and the ranking of A-11 goes down by one place. Such variation in ranking may be attributed to the fact that the fracture toughness of A-4 is inferior compared to A-11, whereas the wear performance of A-4 is superior compared to A-11. Hence, as the weightage of C-6 is increased by +10% and +15%, the ranking of A-4 goes up by one, and as the weightage of C-8 is decreased by −10% and −15%, the ranking of A-11 loses its position by one in the hierarchy of hip implant composites.

4. Conclusions

This study proposed a hybrid multicriteria decision-making framework to solve the problem of selecting the best hip implant composite satisfying a maximum number of preset performance criteria. Thirteen hip implant composites based on a varying proportion of various ceramics (magnesium oxide, zirconium oxide, chromium oxide, silicon nitride and aluminium oxide) were developed and tested for wear and physicomaterial properties. The experimental results of density, void content, hardness, indentation depth, elastic modulus, fracture toughness, compressive strength, and wear were considered as performance criteria in the assessment. With the introduction of AHP method, the weight for each criterion quantified from higher to the lower order as wear (0.340) > fracture toughness (0.227) > elastic modulus (0.111) > hardness (0.108) > compressive strength (0.074) > indentation depth (0.062) > density (0.048) > void content (0.030). By applying MOORA approach, the performance order of hip implant composites could be obtained as A-12 > A-9 > A-3 > A-10 > A-13 > A-4 > A-11 > A-2 > A-8 > A-6 > A-1 > A-7 > A-5. The hip implant alternative A-12 having 83 wt.% of aluminium oxide, 10 wt.% of zirconium oxide, 2.5 wt.% of silicon nitride, 1.5 wt.% of chromium oxide and 3 wt.% of magnesium oxide exhibits optimal wear and physicomaterial properties. Sensitivity analysis shows that a change in criterion weight did not significantly change the overall ranking of the hip implant composite, further enhancing the reliability of the results. The application shows that the proposed AHP-MOORA approach may be used as a trustworthy decision-making framework in selecting hip implant materials along with various decision-making situations and research domains.

Author Contributions: Conceptualization, T.S. and A.P.; Data curation, C.G.; Formal analysis, T.S., C.G., A.P. and L.L.; Investigation, T.S., C.G. and A.P.; Methodology, T.S. and A.P.; Resources, A.P.; Supervision, A.P.; Visualization, L.L.; Writing—original draft, T.S., C.G., A.P. and L.L. All authors have read and agreed to the published version of the manuscript.

Funding: This research received no external funding.

Institutional Review Board Statement: Not applicable.

Informed Consent Statement: Not applicable.

Data Availability Statement: The data that support the findings of this study are available from the first author (T.S.) upon reasonable request.

Acknowledgments: The authors are grateful for the support of CSIR-National Physical Laboratory, New Delhi, India for the spark plasma sintering facility.

Conflicts of Interest: The authors declare no conflict of interest.

References

1. Kurtz, S.; Ong, K.; Lau, E.; Mowat, F.; Halpern, M. Projections of primary and revision hip and knee arthroplasty in the United States from 2005 to 2030. *J. Bone Jt. Surg.* **2007**, *89*, 780–785. [[CrossRef](#)]
2. Khanna, R.; Ong, J.L.; Oral, E.; Narayan, R.J. Progress in Wear Resistant Materials for Total Hip Arthroplasty. *Coatings* **2017**, *7*, 99. [[CrossRef](#)]
3. Derar, H.; Shahinpoor, M. Recent patents and designs on hip replacement prostheses. *Open Bio-Med. Eng. J.* **2015**, *9*, 92. [[CrossRef](#)]
4. Fernández-Fairén, M.; Torres-Perez, A.; Perez, R.; Punset, M.; Molmeneu, M.; Ortiz-Hernández, M.; Manero, J.M.; Gil, J. Early Short-Term Postoperative Mechanical Failures of Current Ceramic-on-Ceramic Bearing Total Hip Arthroplasties. *Materials* **2020**, *13*, 5318. [[CrossRef](#)]

5. Bistolfi, A.; Ferracini, R.; Lee, G.C.; Mellano, D.; Guidotti, C.; Baino, F.; Verné, E. Ceramic-on-ceramic catastrophic liner failure in total hip arthroplasty: Morphological and compositional analysis of fractured ceramic components. *Ceram. Int.* **2021**, *47*, 11029–11036. [[CrossRef](#)]
6. Tun, K.S.; Padnuru Sripathy, A.; Tekumalla, S.; Gupta, M. Development of Novel Lightweight Metastable Metal–(Metal + Ceramic) Composites Using a New Powder Metallurgy Approach. *Materials* **2020**, *13*, 3283. [[CrossRef](#)]
7. Perrichon, A.; Reynard, B.; Gremillard, L.; Chevalier, J.; Farizon, F.; Geringer, J. A testing protocol combining shocks, hydrothermal ageing and friction, applied to Zirconia Toughened Alumina (ZTA) hip implants. *J. Mech. Behav. Biomed. Mater.* **2017**, *65*, 600–608. [[CrossRef](#)]
8. Napier, R.J.; Shimmin, A.J. Ceramic-on-ceramic bearings in total hip arthroplasty: “The future is now”. *Semin. Arthroplast.* **2016**, *27*, 235–238. [[CrossRef](#)]
9. Boutin, P. Experimental study of aluminium in surgery of hip. *Presse Med.* **1971**, *79*, 639–640.
10. Piconi, C.; Sprio, S. Oxide Bioceramic Composites in Orthopedics and Dentistry. *J. Compos. Sci.* **2021**, *5*, 206. [[CrossRef](#)]
11. Iwakiri, K.; Iwaki, H.; Minoda, Y.; Ohashi, H.; Takaoka, K. Alumina inlay failure in cemented polyethylene-backed total hip arthroplasty. *Clin. Orthop. Relat. Res.* **2008**, *466*, 1186–1192. [[CrossRef](#)]
12. Al-Hajjar, M.; Carbone, S.; Jennings, L.M.; Begand, S.; Oberbach, T.; Delfosse, D.; Fisher, J. Wear of composite ceramics in mixed-material combinations in total hip replacement under adverse edge loading conditions. *J. Biomed. Mater. Res. Part B Appl. Biomater.* **2017**, *105*, 1361–1368. [[CrossRef](#)]
13. Rahman, H.S.; Choudhury, D.; Osman, N.A.; Shasmin, H.N.; Abas, W.A. In vivo and in vitro outcomes of alumina, zirconia and their composited ceramic-on-ceramic hip joints. *J. Ceram. Soc. Jpn.* **2013**, *121*, 382–387. [[CrossRef](#)]
14. Jenabzadeh, A.R.; Pearce, S.J.; Walter, W.L. Total hip replacement: Ceramic-on-ceramic. *Semin. Arthroplast.* **2012**, *23*, 232–240. [[CrossRef](#)]
15. Garvie, R.C.; Nicholson, P.S. Structure and thermomechanical properties of partially stabilized zirconia in the CaO-ZrO₂ system. *J. Am. Ceram. Soc.* **1972**, *55*, 152–157. [[CrossRef](#)]
16. Kaivosoja, E.; Tiainen, V.M.; Takakubo, Y.; Rajchel, B.; Sobiecki, J.; Kontinen, Y.T.; Takagi, M. Materials used for hip and knee implants. In *Wear of Orthopaedic Implants and Artificial Joints*; Woodhead Publishing Series in Biomaterials; Woodhead Publishing: Sawston, UK, 2013; pp. 178–218. [[CrossRef](#)]
17. Zhang, Y.; Shu, Y.; Li, W.; Jiang, S.; Cao, W.; Wu, Z.; Wang, K. Effect of MgO doping on properties of low zirconium content Ce-TZP/Al₂O₃ as a joint replacement material. *Ceram. Int.* **2017**, *43*, 2807–2814. [[CrossRef](#)]
18. Shekhawat, D.; Singh, A.; Banerjee, M.K.; Singh, T.; Patnaik, A. Bioceramic composites for orthopaedic applications: A comprehensive review of mechanical, biological, and microstructural properties. *Ceram. Int.* **2021**, *147*, 3013–3030. [[CrossRef](#)]
19. Kobayashi, K.; Kuwajima, H.; Masaki, T. Phase change and mechanical properties of ZrO₂-Y₂O₃ solid electrolyte after ageing. *SolidStateIon* **1981**, *3–4*, 489–493. [[CrossRef](#)]
20. Yoshimura, M.; Noma, T.; Kawabata, K.; Sōmiya, S. Role of H₂O on the degradation process of Y-TZP. *J. Mater. Sci. Lett.* **1987**, *6*, 465–467. [[CrossRef](#)]
21. Chevalier, J.; Gremillard, L.; Deville, S. Low-temperature degradation of zirconia and implications for biomedical implants. *Annu. Rev. Mater. Res.* **2007**, *37*, 1–32. [[CrossRef](#)]
22. Chevalier, J.; Cales, B.; Drouin, J. Low-temperature aging of Y-TZP ceramics. *J. Am. Ceram. Soc.* **1999**, *82*, 2150–2154. [[CrossRef](#)]
23. Colombari, P. Proton conductors and their applications: A tentative historical overview of the early researches. *SolidStateIon* **2019**, *334*, 125–144. [[CrossRef](#)]
24. Schmidt, O.; Gambhir, A.; Staffell, I.; Hawkes, A.; Nelson, J.; Few, S. Future cost and performance of water electrolysis: An expert elicitation study. *Int. J. Hydrog. Energy* **2017**, *42*, 30470–30492. [[CrossRef](#)]
25. Kleiminger, L.; Li, T.; Li, K.; Kelsall, G.H. Syngas (CO-H₂) production using high temperature micro-tubular solid oxide electrolyzers. *Electrochim. Acta* **2015**, *179*, 565–577. [[CrossRef](#)]
26. Arita, M.; Takahashi, Y.; Pezzotti, G.; Shishido, T.; Masoka, T.; Sano, K.; Yamamoto, K. Environmental stability and residual stresses in zirconia femoral head for total hip arthroplasty: In vitro aging versus retrieval studies. *BioMedRes. Int.* **2015**, *2015*, 638502. [[CrossRef](#)]
27. Savin, A.; Craus, M.-L.; Turchenko, V.; Bruma, A.; Dubos, P.-A.; Malo, S.; Konstantinova, T.E.; Burkhovetsky, V.V. Monitoring Techniques of Cerium Stabilized Zirconia for Medical Prosthesis. *Appl. Sci.* **2015**, *5*, 1665–1682. [[CrossRef](#)]
28. Solarino, G.; Spinarelli, A.; Virgilio, A.; Simone, F.; Baglioni, M.; Moretti, B. Outcomes of Ceramic Composite in Total Hip Replacement Bearings: A Single-Center Series. *J. Compos. Sci.* **2021**, *5*, 320. [[CrossRef](#)]
29. Aherwar, A.; Patnaik, A.; Bahraminasab, M.; Singh, A. Preliminary evaluations on development of new materials for hip joint femoral head. *Proc. Inst. Mech. Eng. Part L J. Mater. Des. Appl.* **2019**, *233*, 885–899. [[CrossRef](#)]
30. Bakhsh, A.A. Gamma-Ray Modified Polymer/Clay Composites: Synthesis, Characterization, and Formulation Optimization Using Multivariate Calculus and Graph Theory. *Energies* **2021**, *14*, 2724. [[CrossRef](#)]
31. Shevtsov, S.; Zhilyaev, I.; Chang, S.-H.; Wu, J.-K.; Snezhina, N. Multi-Criteria Decision Approach to Design a Vacuum Infusion Process Layout Providing the Polymeric Composite Part Quality. *Polymers* **2022**, *14*, 313. [[CrossRef](#)]
32. Singh, T. Utilization of cement bypass dust in the development of sustainable automotive brake friction composite materials. *Arab. J. Chem.* **2021**, *14*, 103324. [[CrossRef](#)]

33. Paul, A.; Shukla, N.; Paul, S.K.; Trianni, A. Sustainable Supply Chain Management and Multi-Criteria Decision-Making Methods: A Systematic Review. *Sustainability* **2021**, *13*, 7104. [[CrossRef](#)]
34. Bączkiewicz, A.; Kizielewicz, B.; Shekhovtsov, A.; Wątróbski, J.; Sałabun, W. Methodical Aspects of MCDM Based E-Commerce Recommender System. *J. Theor. Appl. Electron. Commer. Res.* **2021**, *16*, 2192–2229. [[CrossRef](#)]
35. Singh, T. Optimum design based on fabricated natural fiber reinforced automotive brake friction composites using hybrid CRITIC-MEW approach. *J. Mater. Res. Technol.* **2021**, *14*, 81–92. [[CrossRef](#)]
36. Simic, V.; Gokasar, I.; Deveci, M.; Karakurt, A. An integrated CRITIC and MABAC based type-2 neutrosophic model for public transportation pricing system selection. *Socio-Econ. Plan. Sci.* **2022**, *80*, 101157. [[CrossRef](#)]
37. Singh, T. A hybrid multiple-criteria decision-making approach for selecting optimal automotive brake friction composite. *Mater. Des. Processing Commun.* **2021**, *3*, e266. [[CrossRef](#)]
38. Akkaya, G.; Turanoğlu, B.; Öztas, S. An integrated fuzzy AHP and fuzzy MOORA approach to the problem of industrial engineering sector choosing. *Expert Syst. Appl.* **2015**, *42*, 9565–9573. [[CrossRef](#)]
39. Indrajayanthan, V.; Mohanty, N.K. Assessment of Clean Energy Transition Potential in Major Power-Producing States of India Using Multi-Criteria Decision Analysis. *Sustainability* **2022**, *14*, 1166. [[CrossRef](#)]
40. Goswami, C.; Bhat, I.K.; Bathula, S.; Singh, T.; Patnaik, A. Physico-mechanical and surface wear assessment of magnesium oxide filled ceramic composites for hip implant application. *Silicon* **2019**, *11*, 39–49. [[CrossRef](#)]
41. Aragón-Duarte, M.C.; Nevarez-Rascón, A.; Esparza-Poncea, H.E.; Nevarez-Rascón, M.M.; Talamantes, R.P.; Ornelasa, C.; Mendez-Nonella, J.; González-Hernández, J.; Yacamán, M.J.; Hurtado-Macías, A. Nanomechanical properties of zirconia- yttria and alumina zirconia- yttria biomedical ceramics, subjected to low temperature aging. *Ceram. Int.* **2017**, *43*, 3931–3939. [[CrossRef](#)]
42. Oliver, W.C.; Pharr, G.M. An improved technique for determining hardness and elastic modulus using load and displacement sensing indentation experiments. *J. Mater. Res.* **1992**, *7*, 1564–1583. [[CrossRef](#)]
43. Anstis, G.R.; Chantikul, P.; Lawn, B.R.; Marshall, D.B. A critical evaluation of indentation techniques for measuring fracture toughness: I, direct crack measurements. *J. Am. Ceram. Soc.* **1981**, *64*, 533–538. [[CrossRef](#)]
44. Goswami, C.; Bhat, I.K.; Patnaik, A.; Singh, T.; Fekete, G. Fabrication of Ceramic Hip Implant Composites: Influence of silicon nitride on physical, mechanical and wear properties. *Silicon* **2020**, *12*, 1237–1245. [[CrossRef](#)]
45. ISO-23317; Implants for Surgery-In Vitro Evaluation for Apatite-Forming Ability of Implant Materials. International Organization for Standardization: Geneva, Switzerland, 2007.
46. Harnpornchai, N.; Wonggattaleekam, W. An Application of Neutrosophic Set to Relative Importance Assignment in AHP. *Mathematics* **2021**, *9*, 2636. [[CrossRef](#)]
47. Singh, T.; Patnaik, A.; Fekete, G.; Chauhan, R.; Gangil, B. Application of hybrid analytical hierarchy process and complex proportional assessment approach for optimal design of brake friction materials. *Polym. Compos.* **2019**, *40*, 1602–1608. [[CrossRef](#)]
48. Brauers, W.K.M. Multi-objective seaport planning by MOORA decision making. *Ann. Oper. Res.* **2013**, *206*, 39–58. [[CrossRef](#)]
49. Brodny, J.; Tutak, M. Analyzing the Level of Digitalization among the Enterprises of the European Union Member States and Their Impact on Economic Growth. *J. Open Innov. Technol. Mark. Complex.* **2022**, *8*, 70. [[CrossRef](#)]
50. Gupta, K.; Roy, S.; Poonia, R.C.; Kumar, R.; Nayak, S.R.; Altameem, A.; Saudagar, A.K.J. Multi-Criteria Usability Evaluation of mHealth Applications on Type 2 Diabetes Mellitus Using Two Hybrid MCDM Models: CODAS-FAHP and MOORA-FAHP. *Appl. Sci.* **2022**, *12*, 4156. [[CrossRef](#)]
51. Li, W.; Gao, L. Rapid sintering of nanocrystalline ZrO₂(3Y) by spark plasma sintering. *J. Eur. Ceram. Soc.* **2000**, *20*, 2441–2445. [[CrossRef](#)]
52. Mazzocchi, M.; Gardini, D.; Traverso, P.L.; Faga, M.G.; Bellosi, A. On the possibility of silicon nitride as a ceramic for structural orthopaedic implants. Part II: Chemical stability and wear resistance in body environment. *J. Mater. Sci. Mater. Med.* **2008**, *19*, 2889. [[CrossRef](#)]
53. Zhang, C.; Wang, F.; Jiang, Z.; Lan, J.; Zhao, L.; Si, P. Effect of graphene oxide on the mechanical, tribological, and biological properties of sintered 3Y-ZrO₂/GO composite ceramics for dental implants. *Ceram. Int.* **2021**, *5*, 6940–6946. [[CrossRef](#)]
54. Bull, S.J.; Moharrami, N.; Langton, D. Mechanistic study of the wear of ceramic heads by metallic stems in modular implants. *J. Bio-Tribo-Corros.* **2017**, *3*, 7. [[CrossRef](#)]
55. Sedlák, R.; Ivor, M.; Klimczyk, P.; Wyzga, P.; Podsiadlo, M.; Vojtko, M.; Dusza, J. Micro/Nano Indentation Testing of Spark Plasma Sintered Al₂O₃ + ZrO₂ + cBN Ceramics. *Ceramics* **2021**, *4*, 40–53. [[CrossRef](#)]
56. Benavente, R.; Salvador, M.D.; Penaranda-Foix, F.L.; Pallone, E.; Borrell, A. Mechanical properties and microstructural evolution of alumina-zirconia nanocomposites by microwave sintering. *Ceram. Int.* **2014**, *40*, 11291–11297. [[CrossRef](#)]
57. Sarker, S.; Mumu, H.T.; Al-Amin, M.; Alam, M.Z.; Gafur, M.A. Impacts of inclusion of additives on physical, microstructural, and mechanical properties of Alumina and Zirconia toughened alumina (ZTA) ceramic composite: A review. *Mater. Today Proc.* **2021**, in press. [[CrossRef](#)]
58. Arab, A.; Sktani, Z.D.I.; Zhou, Q.; Ahmad, Z.A.; Chen, P. Effect of MgO Addition on the Mechanical and Dynamic Properties of Zirconia Toughened Alumina (ZTA) Ceramics. *Materials* **2019**, *12*, 2440. [[CrossRef](#)]
59. Riu, D.-H.; Kong, Y.-M.; Kim, H.-E. Effect of Cr₂O₃ addition on microstructural evolution and mechanical properties of Al₂O₃. *J. Eur. Ceram. Soc.* **2000**, *20*, 1475–1481. [[CrossRef](#)]
60. Heimann, R.B. Silicon Nitride, a Close to Ideal Ceramic Material for Medical Application. *Ceramics* **2021**, *4*, 208–223. [[CrossRef](#)]

61. Gallo, J.; Goodman, B.S.; Lostak, J.; Janout, M. Advantages and disadvantages of ceramic on ceramic total hip arthroplasty: A review. *Biomed. Pap.* **2012**, *156*, 204–212. [[CrossRef](#)]
62. Harding, D.; Loesener, G.; Ngyuen, B.; Blackburn, D.; Dixon, R.; Taylor, J. Comparison of Wear for Polycrystalline Diamond, Cobalt Chrome, and Polyethylene in a High Hertzian Stress Environment. *Orthop. Proc.* **2018**, *94-B*, SUPP_XL.
63. Amaral, M.; Maru, M.M.; Rodrigues, S.P.; Gouvêa, C.P.; Trommer, R.M.; Oliveira, F.J.; Achete, C.A.; Silva, R.F. Extremely low wear rates in hip joint bearings coated with nanocrystalline diamond. *Tribol. Int.* **2015**, *89*, 72–77. [[CrossRef](#)]